Preprints of the 19th World Congress
The International Federation of Automatic Control
Cape Town, South Africa. August 24-29, 2014

Modelling PV Clouding Effects Using a Semi-Markov Process with Application to Energy Storage

Arthur K. Barnes*, Juan C. Balda**
Jonathan K. Hayes***

** University of Arkansas, Electrical Engineering Department, Fayetteville, AR 72701 USA (Tel: 479-530-8117; e-mail: artbarnes@ ieee.org).*
*** University of Arkansas, Electrical Engineering Department, Fayetteville, AR 72701 USA (e-mail:jbalda@uark.edu)*
**** University of Arkansas, Electrical Engineering Department, Fayetteville, AR 72701 USA (e-mail: jkhayes12@gmail.com)*

Abstract: Cloud-induced intermittency of photovoltaic (PV) generation forces equipment on the electrical grid to cycle excessively preventing PV from being considered as a reliable or dispatchable source of power. Energy storage units (ESU) are proposed to turn PV power dispatchable. In order to use an ESU most effectively, it must be controlled appropriately by considering cloud-induced effects. To this end, the cloud structure is modeled as a random sequence inferred from clouding data. The proposed model is valid for centralized PV installations and serves to develop not only a control methodology to coordinate an ESU with existing grid equipment but also as a sizing criterion for an ESU. The above methodology is demonstrated on both clouding data collected from a rooftop PV installation that includes a pyranometer.

1. INTRODUCTION

Improvements in the manufacturing process of PV generation are lowering costs and leading to increased grid penetration. However, the power output of PV inverters varies sharply because of changing cloud cover that may cause transitions from rated power to less than half of rated power within minutes (Hill et al., 2012). This may cause over- or under-voltages on distribution systems (Shayani and de Oliveira, 2011; Barnes et al., 2012) in addition to reducing the maintenance interval of voltage regulating equipment such as substation load tap-changers (LTC) or in-line voltage regulators (Liu et al., 2012).

Energy storage has long been proposed as a solution; however, it is necessary to either model or predict cloud-induced intermittency to develop a more-efficient ESU control strategy (Chen et al., 2012; Liang and Liao, 2007; Omran et al., 2011; Song et al., 2012). Frequency-domain methods have been previously applied to characterize PV power (Vetterling, 1992). Unfortunately, the resulting frequency-domain signal has units without physical significance (Taylor and Mellott, 1998). Despite these methods being useful for observing qualitative features of PV power intermittency, they not suitable for sizing ESU which requires knowledge of the peak energy amount charged to or discharged from a battery.

Methods for control of the ESU include deterministic scheduling, stochastic scheduling, rule-based control, feedback control, and feedforward control (Chen et al., 2012; Korpas and Holen, 2006; Liang and Liao, 2007; Liu et al., 2012; Omran et al., 2011), with deterministic scheduling employed most commonly. Prediction of PV power is necessary for ESU control methods based on deterministic scheduling (Korpas and Holen, 2006), and has received significant attention in recent years. Current methods are divided into two major groups (Lorenz et al., 2009). The first group consists of those methods using numerical weather prediction to estimate hourly averaged power with look-ahead intervals on the order of one or more days (Anvari Moghaddam and Seifi, 2011). The second group of methods uses sky imagers, geographically distributed sensor arrays, or satellite imagery to track cloud position over time (Bing et al., 2012; Lonij et al., 2012; Stefferud et al., 2012). This yields power predictions on the order of a few hours ahead (Rikos et al., 2008). The time resolution for both methods are too coarse for predicting cloud-induced power variations, which occurs in seconds (Stefferud et al., 2012).

The contributions of this work are a random-sequence model for cloud-induced intermittency in a single PV installation, and its application to develop an efficient rule-based ESU control strategy. The model is applicable to large, central PV installations that form 38% of installed PV generation (Sherwood, 2012). Unlike frequency-domain methods, the model outputs have physical units. The control strategy requires neither sky imaging data nor remote irradiance measurements, unlike existing methods. Additionally, both the model and rule-based controller operate over time scales on the order of seconds, suitable for modelling and mitigating the effects of cloud-induced intermittency. The model is also useful for generating simulated test data, similar to the case of wind generation, where either the Weibull distribution or time-series models are used.

This paper is organized as follows: the PV data collection is described in section 2; the data processing is explained in section 3; the data analysis and development of statistical distributions are addressed ins section 4; the reward process

used to develop a control policy is described in section 5; the results of the methodology applied to a case study are presented in section 6; and lastly, the conclusions on the work performed as well as directions for future work are given in section 7.

2. PV DATA ACQUISITION

Irradiance is captured with an irradiance sensor (Apogee SP-125 5V amplified pyronameter (Apogee Instruments, 2011) in conjunction with a LabVIEW-based data acquisition system (National Instruments USB-6259) using a custom program. The pyranometer is installed at the University of Arkansas (UA) in Fayetteville (AR) on the top of the John A. White Engineering Hall roof next to a pair of 225 W PV panels as shown in Fig. 1. It was installed on the same plane as the panels, facing South with tilt angle of 66º from horizontal. The PV data are available on the web at http://energy.uark.edu/pv.

An unanswered question for PV generation systems is that of sample rate selection. Notably, very wide ranges of sample rates abound, including 3 seconds (NREL, 2011) to 1 hour (NREL, 2011). The authors sought to select a sample rate that preserved the salient characteristics of cloud-induced intermittency. The system supports sample rates of up to 25 Hz with the sample rate selected on the theoretical frequency content of the irradiance sensor output voltage and inspection of recorded data. The 25 Hz maximum sample rate of the data acquisition system was determined to be sufficient, and data was initially collected at this rate. However, this sample rate results in prohibitively large amounts of data over long periods of time.

Moreover, it is only necessary in this application to detect the presence of large changes in irradiance, those where the irradiance changes by 70% of the maximum irradiance value or more (Grady and Libby, 2012). Visual inspection revealed that the time duration between peaks in the irradiance profile meeting this criteria was usually 2.5 s or more. Hence, the selected final sample rate selection is 1 Hz.

3. PV DATA PROCESSING

Erroneous values corrupted by noise and nonlinear effects in the sensor are unfortunately captured by the data acquisition system. Hence, the data must be processed to remove these erroneous values that occur at low irradiance as well as to capture statistics on clouding. This processing classifies data as *clear* or *shaded*, using the algorithm described in Fig. 2.

Convergence is established within 3 iterations, so a convergence check was not implemented. The algorithm works by alternately estimating the clear-sky irradiance profile using a second-order curve fit and classifying the data as *clear* or *shaded*. Note that for PV systems with tracking, the irradiance profile will be flattened near mid-day (Seme et al., 2011), so a higher-order curve fit will be necessary. Each value is divided by the clear-sky irradiance profile at the corresponding time. The resulting values are clustered using K-means clustering with two centroids (Duda et al., 2001). Each subsequent clustering results in a more refined estimate of the clear-sky irradiance profile. Fig. 3 shows the classification results.

The processing accomplishes two goals: First, the data are classified as either *clear* or *shaded*, allowing for statistics to be taken on cloud cover. Second, it mitigates corrupted data by removing erroneous samples and interpolating between the remaining good data. For the case of the pyranometer, two factors were observed to corrupt data. First, accuracy at high solar angles of incidence is poor as the output drops off. Second, oscillation is present at those high angles of incidence, illustrated around 6 am and 7 pm (19 h) in Fig. 3, which compares the measured and corrected data To overcome these issues, the corrupted samples are removed and a weighted sum of the predicted and measured irradiance is used to estimate the true irradiance.

Fig. 1. Experimental setup at UA.

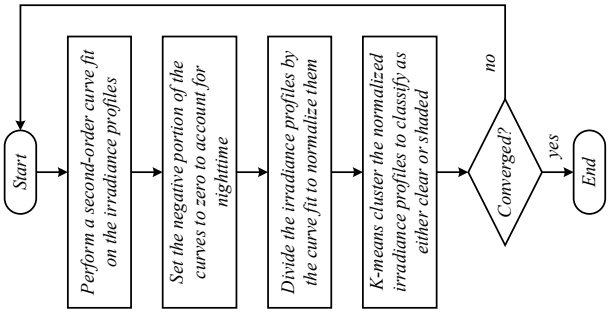

Fig. 2. Flowchart for the classification algorithm.

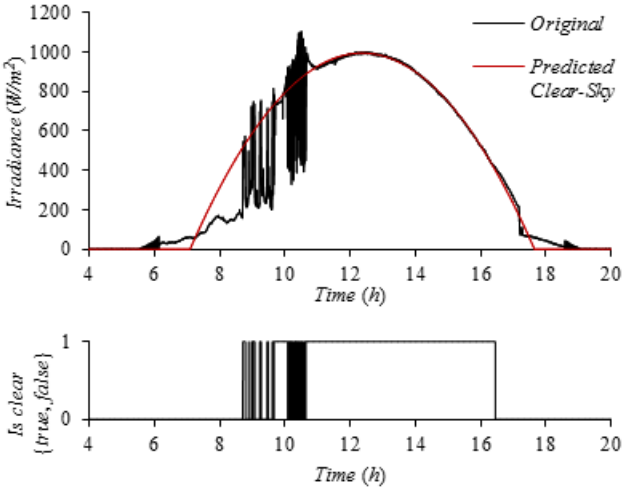

Fig. 3. Classified irradiance data for a partly cloudy day (Aug 27, 2011). The original irradiance profile and predicted clear-sky irradiance profile are in the top graphs, while the classification results (whether or not it is clear or shaded) are in the bottom graph.

4. Exploratory Data Analysis and Statistical Inference of Cloud Durations

In order to characterize and forecast the PV output, it is assumed that the *clear* and *shaded* durations follow statistical distributions. Based on existing work in climate science (Neggers et al., 2003), cumulus clouds have a fractal structure, so the distribution of the cloud size x, and thus the duration of shading t, follow a power law distribution

$$f(x) = Ax^b, \tag{1}$$

where A and b are distribution parameters. Through exploratory data analysis, it is inferred that the *clear* and *shaded* distributions follow a generalized Pareto distribution of the form

$$f(t|k,\sigma,\theta) = \frac{1}{\sigma}\left[1 + k\frac{(t-\theta)}{\sigma}\right]^{-1-\frac{1}{k}}, \tag{2}$$

where k, σ, θ are parameters of the distribution. Although the duration of *clear* conditions is truncated based on the length of a day, the effect of truncation is neglected. Two separate distributions are inferred for the duration of *clear* and *shaded* events, respectively. Quantile-quantile (QQ) plots are used to evaluate how the fitted distributions handle outliers, illustrated in Fig. 4. In these figures, the inverse cumulative distribution functions (CDF) of the inferred distributions are plotted against the observed values for *clear* and *shaded* durations. The better the inferred distribution fits the data, the more the plotted points fall on the line $y = x$. The inferred distributions fit the data well with the exception that the distribution of *shaded* durations is more long-tailed than the observed data, and quantization occurs at small time scales.

5. Applicability of Clouding Distributions To ESU

The characterization of the distribution of the *clear* and *shaded* durations, as well as the likelihood that the PV installation will be *clear* or *shaded* at a given time in the future are necessary to develop an ESU control strategy or sizing criterion.

The state of the PV installation is modelled as a time series $s_1, s_2, \ldots s_N$, where each at sample n, the state s_n is either 1, denoting *clear*, or 2, denoting *shaded*. Part 4 revealed that s_n is dependent not just on s_{n-1}, but also on the total duration that the sensor has been *clear* or *shaded*, thereby violating the Markov property (Duda et al., 2001). This is apparent because the distributions of the *clear* and *shaded* events are not exponential, which is required for the Markov property to hold (Duda et al., 2001). Next, it is shown that the distributions of *clear* and *shaded* times can still be used to model the shading as a discrete-time semi-Markov process (Howard, 2007).

5.1. Semi-Markov Discrete-Time Process Model

A Markov process has a set of states and a state-transition probability matrix indicating the likelihood p_{ij} of transitioning from state i to state j at sample n (Feller, 2008; Papoulis and Pillai, 2002; Sharma, 2009). The semi-Markov discrete-time process (SMDTP) is a generalization of the Markov process that waits for a random hold time before each transition. Therefore, each element p_{ij} of the SMDTP state-transition probability matrix has a corresponding hold time distribution $h_{ij}(m)$. When a SMDTP has transitioned to state i, it randomly selects the next state j based on the p_{ij}. In the discrete-time case addressed here, the selection is based on $h_{ij}(m)$, the number of samples m to wait before transitioning to state j.

Irradiance is modelled by a two-state model in which virtual state transitions are forbidden (that is, transitions from a state to itself), illustrated in Fig. 5. This results in a simpler representation of the system, as the state-transition probability matrix is simply a two-by-two identity matrix. The SMDTP can be executed via the algorithm described in Fig. 6 in order to generate simulated data.

For forecasting, the quantities of interest are the interval transition probabilities, giving the likelihood that the PV is *clear* or *shaded* at sample n given that it transitioned to be *clear* or *shaded* at sample 0. The interval transition probability $\phi_{ij}(n)$ is the probability that the process is in state i at sample n, given that it entered state j at sample 0; in particular

$$\phi_{12}(n) = \sum_{n=0}^{N}\sum_{m=1}^{n} h_{12}(m)\phi_{22}(n-m). \tag{3}$$

$$\phi_{21}(n) = \sum_{n=0}^{N}\sum_{m=1}^{n} h_{21}(m)\phi_{11}(n-m). \tag{4}$$

Again, the term $h_{ij}(m)$ is the probability that the process will transition into state i at sample m given that it entered state j at sample 0. Because these calculations rely on a series of multiply-accumulate operations which are performed quickly by modern computers, they are easily computed numerically using the following initial conditions

$$\Phi(0) = \begin{bmatrix} 1 & 0 \\ 0 & 1 \end{bmatrix} \tag{5}$$

and the definition of a probability mass function

$$\phi_{11}(n) + \phi_{21}(n) = 1 \tag{6}$$

$$\phi_{12}(n) + \phi_{22}(n) = 1, \tag{7}$$

where (5) reflects the fact that at sample 0 the state of the process is known as it has just been observed.

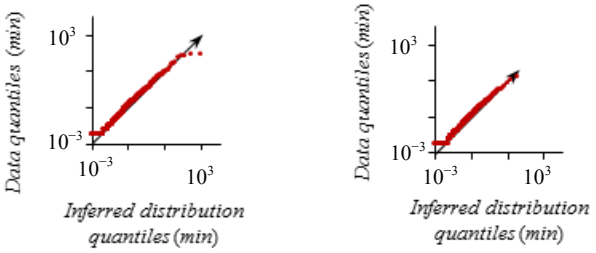

(a) (b)

Fig. 4. QQ plot of shaded durations comparing the distribution against data.

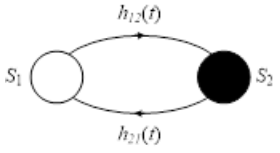

Fig. 5. Graphical illustration of the SMDTP model.

The interval transition probabilities allow for performing forecasting by taking the state with the highest likelihood. For example, if a process transitioned from *clear* to *shaded* at sample 0, it will most likely remain shaded for 50 seconds until $\phi_{21}(n)$ exceeds 0.5, as illustrated by Fig. 7. This figure illustrates the evolution of the interval transition probabilities over time assuming that the system started in *clear* (state 1, red lines), or *shaded* (state 2, black lines). As time increases, the uncertainty in the interval transition probabilities increases and they converge to their steady-state values, the marginal likelihood of the system being either *clear* or *shaded*.

5.2. Voltage Variations Caused by PV Intermittency

The variations in voltage caused by intermittency of PV generation on the feeder are calculated as follows. It is assumed that the feeder can be modelled as a voltage source behind an equivalent series impedance (Shayani and de Oliveira, 2011), illustrated in Fig. 8. Using the notation in (Baran and Wu, 1989), the voltage magnitude as function of real and reactive power injections is

$$V_{pv}^2 = V_\infty^2 + 2(RP + XQ) - \frac{Z^2}{V_{pv}^2}(P^2 + Q^2) \tag{8}$$

$$P = P_{pv} + P_{esu} - P_{load} \tag{9}$$

$$Q = -Q_{load}. \tag{10}$$

In the above, R and X are the resistive and reactive portions of the line impedance while P and Q are the real and reactive powers flowing into the PV bus at the end of the line. The real power is broken up into the PV real power injection P_{pv}, ESU real power injection P_{esu}, and load real power draw P_{load}. The reactive power consists only of the load reactive power draw Q_{load}. For notational convenience, V_∞, V_{pv} and Z are defined as the magnitudes of the infinite bus voltage, PV installation bus voltage, and equivalent series impedance.

The change in voltage magnitude with respect to real power injection is

$$J = \frac{\partial V_{pv}}{\partial P} = \frac{-2V_{pv}^2 + 2Z^2P}{4V_{pv}^2 + (2RP - 2V_\infty^2)V_{pv}}. \tag{11}$$

It is assumed that the substation LTC has T taps allowing for a total variation of $\pm\Delta V$ V from nominal. Assuming voltage sensing at the PV bus, the amount of voltage variation required for the LTC to cycle is therefore $\pm 2\Delta V/T$ V. This corresponds to a change in power of

$$P_{tap} = \pm 2\Delta V/(TJ). \tag{12}$$

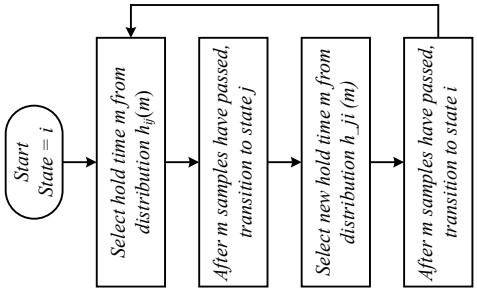

Fig. 6. Simulation of the SMDTP.

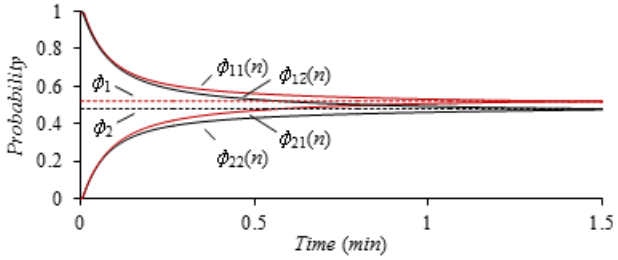

Fig. 7. Interval transition probabilities $\phi_{ij}(n)$ converging to the steady-state probabilities ϕ_i. The probabilities $\phi_1 + \phi_2 = 1$.

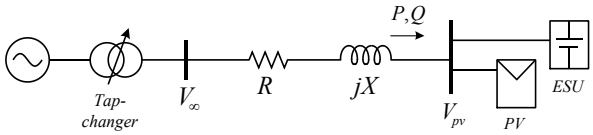

Fig. 8. Equivalent feeder model with transformer LTC, PV generation and ESU.

5.3. Reward Model

Two reward processes are used to calculate both the number of LTC tap-changes and the ESU battery throughput. These two quantities are considered the rewards to be determined, though they are actually costs. Similar to the case of the interval transition probabilities, the reward processes are calculated recursively as follows

$$v_1(n) = {}^{>}y_1(n) + r_1(n) + \sum_{m=1}^{n} h_{21}(n)\, v_2(n-m) \tag{13}$$

$$v_2(n) = {}^{>}y_2(n) + r_2(n) + \sum_{m=1}^{n} h_{12}(n)\, v_1(n-m) \tag{14}$$

$${}^{>}y_1(n) = y_1(n,1) \sum_{m=n+1}^{\infty} h_{12}(m) \tag{15}$$

$${}^{>}y_2(n) = y_2(n,1) \sum_{m=n+1}^{\infty} h_{21}(m) \tag{16}$$

$$r_1(n) = \sum_{m=1}^{n} h_{12}(n)\, y_1(n,1) \tag{17}$$

$$r_2(n) = \sum_{m=1}^{n} h_{21}(n)\, y_2(n,1) \tag{18}$$

$$y_i(m,1) = \sum_{l=0}^{m-1} y_{i,x}(l) \tag{19}$$

$$y_{i,tc}(l) = \begin{cases} 1, & l = n_{sw} \\ 0, & otherwise \end{cases} \tag{20}$$

$$y_{i,esu}(l) = \begin{cases} \Delta E_{esu}, & i = 2 \text{ and } l \le n_{sw} \\ 0, & otherwise \end{cases} \tag{21}$$

These assume zero initial rewards, so $v_i(0) = 0$. The significances of the terms are as follows: $v_i(n)$ is the expected reward of the process at sample n given that the process entered state i at sample 0. The term ${}^{>}y_i(n)$ is the expected reward conditioned on the event that the process

transitions to another state after sample n. The term $r_i(n)$ is the expected reward that the process earns in state i, conditioned on the event that the process transitions to another state before sample n. The last terms in (13) and (14) are the expected rewards earned over samples $n-m$ to n conditioned on the event that the process transitions to another state before sample n. The term $y_i(m,1)$ represents the cumulative reward accrued over m samples. The term $y_{i,x}(l)$ is the reward rate at l samples after having transitioned into state i. In this case the reward is actually a cost. Two reward rates are considered. The rate, $y_{i,tc}(l)$ is the number of tap-changes that occur, while $y_{i,esu}(l)$ is the battery throughput. These assume that a tap-change will occur when a timeout period equal to n_{sw} samples has elapsed after the process has changed states. During those n_{sw} samples, the ESU will either supply or draw a fixed amount of power to regulate voltage. Only discharge power is considered in calculating battery throughput. The two costs are used to select the timeout period that minimizes the ESU throughput while maintaining the expected number of tap-changes per day within the allowable maximum.

6. Methodology Results

The objective is to assess the necessary amount of energy storage and develop a control strategy to avoid excessive cycling of a LTC. The selected strategy is for the ESU to fill in dips in power until a timeout counter expires. The SMDTP is used to select the timeout parameter. For this analysis, one-minute data taken on May 1, 2013 from the 15 kW Fayetteville (AR) Public Library PV installation is studied. The inferred parameters for the *clear* and *shaded* durations are illustrated in Table I. These parameters are applied to study a 2 MW PV installation illustrated in Fig. 8. It uses the feeder parameters from (Shayani and de Oliveira, 2011) and the additional parameters specified in Table II. Both the ESU and PV are approximated as ideal ac current sources (assuming only small changes in V_{pv} in Fig. 8. Based on the desired lifetime of the transformer/LTC, the ESU control strategy must limit the number of tap changes per day to

$$O_{day} = \frac{N_{life}}{365 \times Y_{life}} = \frac{3 \times 10^5}{365 \times 40} = 20. \qquad (22)$$

Given the feeder parameters, a load-flow analysis indicates a 1.27% voltage rise per MW. For an LTC with the parameters in Table II, the power change for a tap-change is $P_{tap} = (2\Delta V)/(TJ) = (2 \cdot 0.01)/(32 \cdot 0.0127) = 489$ kW.

Based on previous work in cloud intermittency, a typical cloud will result in the power output decreasing to 30% of clear-sky conditions (Grady and Libby, 2012).

Thus, the minimum necessary clear-sky output power in kW need for the PV to induce a tap-change during clouding is

$$\check{P}_{pv} = P_{tap}/\alpha = 489/0.7 = 689. \qquad (23)$$

Based on the collected data, the duration during the studied day that the 2 MW PV generation can cause a tap-change $\check{t}_{pv}$ and the average change in PV power during clouding $\Delta\bar{P}_{pv}$ are calculated and given in Table III. These figures are used to calculate the battery capacity.

By sweeping the ESU timeout, the corresponding ESU throughput at 20 tap-changes per day is 2.625 MWh, using a zero-order approximation of ESU power (ESU power is approximated by the average power in the reward calculations). However, the actual discharge durations are at most equal to the selected ESU timeout corresponding to 20 minutes. Fig. 9 illustrates the number of tap-changes and the battery throughput over the course of a day with the selected control parameters. Fig. 10 shows a snapshot of the ESU charge/discharge schedule as the ESU compensates for cloud-induced intermittency.

TABLE I. DISTRIBUTIONS OF CLEAR AND SHADED DURATIONS

		K	σ	θ
Irradiance Sensor	*Clear*	1.798	3.808×10^{-3}	10^{-4}
	shaded	1.206	3.452×10^{-3}	10^{-4}
PV Power	*Clear*	0.367	0.231	10^{-4}
	shaded	0.056	0.0631	10^{-4}

TABLE II. STUDY PARAMETERS

Component	*Parameter*	*Expression*	*Value*
PV	*Rated power*	$\hat{P}_{pv}$	2 MW
Transformer	*Desired lifetime*	Y_{life}	40 years
LTC	*Lifetime operations*	O_{life}	3×10^5
	Regulation range	ΔV	10%
	LTC steps	T	32
PV	*Cloud-induced power reduction*	α	70%

TABLE III. STUDY RESULTS

Component	*Parameter*	*Expression*	*Value*
Feeder	*Change in net power required to induce a tap-change*	P_{tap}	489 kW
PV	*Minimum PV output power for a tap-change to occur during clouding*	$\check{P}_{pv}$	698 kW
	Time during studied day that $P_{pv} \geq \check{P}_{pv}$	$\check{t}_{pv}$	11.6 h
	Average PV power while $P_{pv} \geq \check{P}_{pv}$	$\bar{P}_{pv}$	1.5 MW
	Average change in power during clouding while $P_{pv} \geq \check{P}_{pv}$	$\Delta\bar{P}_{pv}$	1.05 MW
ESU	*ESU timeout*	t_{sw}	*20* minutes
	Average ESU output power while $P_{pv} \geq \check{P}_{pv}$	$\bar{P}_{esu}$	525 kW
	Daily ESU energy throughput	E_{day}	2.625 MWh

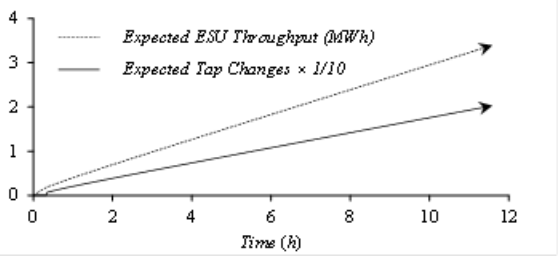

Fig. 9. Expected number of tap-changing operations and ESU throughput vs. time.

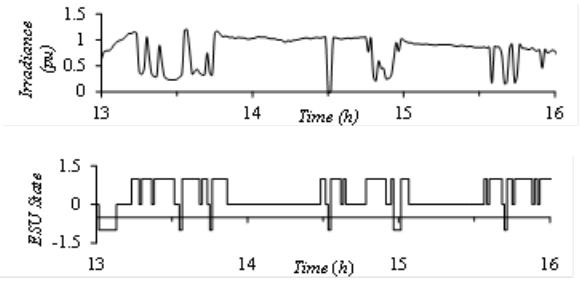

Fig. 10. Irradiance vs. time and ESU state vs. time. A value of +1 indicates discharging, –1 indicates charging, and 0 indicates standby.

7. CONCLUSIONS

A SMDTP model was proposed to fit observed clouding data. The model was most useful for selecting a control strategy offline because the conditional probabilities of *clear* and *shaded* future states converge to their steady-state values rapidly, though conditioning on weather data offers the potential for improved performance. It was applied to calculate the expected number of tap-changes and battery throughput for an ESU coordinated with a transformer LTC in order to select a control strategy and battery capacity. The results demonstrate how the proposed method allows for LTC maintenance intervals to be met while minimizing battery utilization in an ESU.

REFERENCES

Anvari Moghaddam, A., Seifi, A.R., 2011. Study of forecasting renewable energies in smart grids using linear predictive filters and neural networks. IET Renew Power Gener 5, 470 –480.

Apogee Instruments, 2011. Pyranometer SP-212 & 215 [WWW Document]. URL http://www.apogeeinstruments.com/manuals/SP-212_215manual.pdf (accessed 7.21.11).

Baran, M., Wu, F.F., 1989. Optimal sizing of capacitors placed on a radial distribution system. IEEE Trans Power Del 4, 735–743.

Barnes, A.K., Balda, J.C., Escobar-Mejia, A., Geurin, S.O., 2012. Placement of energy storage coordinated with smart PV inverters, in: IEEE PES ISGT. pp. 1–7.

Bing, J., Bartholomy, O., Krishnani, P., 2012. Validation of solar PV power forecasting methods for high penetration grid integration, in: IEEE Power and Energy Society General Meeting. pp. 1–6.

Chen, S.X., Gooi, H.B., Wang, M.Q., 2012. Sizing of energy storage for microgrids. *IEEE Trans. Smart Grid 3*, 142–151.

Duda, R.O., Hart, P.E., Stork, D.G., 2001. Pattern classification. Wiley.

Feller, W., 2008. An Introduction to Probability: Theory and its Applications, 3rd ed. Wiley India Pvt. Limited.

Grady, W.M., Libby, L., 2012. A cloud shadow model and tracker suitable for studying the impact of high-penetration PV on power systems, in: IEEE Energytech. pp. 1–6.

Hill, C.A., Such, M.C., Chen, D., Gonzalez, J., Grady, W.M., 2012. Battery energy storage for enabling integration of distributed solar power generation. *IEEE Trans. Smart Grid 3*, 850–857.

Howard, R.A., 2007. Dynamic Probabilistic Systems: Markov Models, Dover Books on Mathematics Series. Dover Publications, Incorporated, Mineola, NY.

Korpas, M., Holen, A.T., 2006. Operation planning of hydrogen storage connected to wind power operating in a power market. IEEE Trans. on Energy Convers. On 21, 742–749.

Liang, R.-H., Liao, J.-H., 2007. A fuzzy-optimization approach for generation scheduling with wind and solar energy systems. *IEEE Trans. Power Syst. 22*, 1665–1674.

Liu, X., Aichhorn, A., Liu, L., Li, H., 2012. Coordinated control of distributed energy storage system with tap changer transformers for voltage rise mitigation under high photovoltaic penetration. *IEEE Trans. Smart Grid 3*, 897–906.

Lonij, V.P.A., Jayadevan, V.T., Brooks, A.E., Rodriguez, J.J., Koch, K., Leuthold, M., Cronin, A.D., 2012. Forecasts of PV power output using power measurements of 80 residential PV installs, in: 38th IEEE Photovoltaic Specialists Conference (PVSC). pp. 003300 –003305.

Lorenz, E., Hurka, J., Heinemann, D., Beyer, H.G., 2009. Irradiance forecasting for the power prediction of grid-connected photovoltaic systems. *IEEE J. Sel. Top. Appl. Earth Obs. 2*, 2 – 10.

Neggers, R., Jonker, H., Siebesma, A., 2003. Size statistics of cumulus cloud populations in large-eddy simulations. *J. Atmospheric Sci. 60*, 1060–1074.

National Renewable Energy Laboratory, 2011. NREL: Measurement and Instrumentation Data Center (MIDC) Home Page [WWW Document]. URL http://www.nrel.gov/midc/ (accessed 11.30.11).

Omran, W.A., Kazerani, M., Salama, M.M.A., 2011. Investigation of methods for reduction of power fluctuations generated from large grid-connected photovoltaic systems. *IEEE Trans. Energy Convers. 26*, 318–327.

Papoulis, A., Pillai, S.U., 2002. Probability, Random Variables, and Stochastic Processes. Tata McGraw-Hill.

E. Rikos, S. Tselepis, C. Hoyer-Klick, and M. Schroedter-Homscheidt, "Stability and power quality issues in microgrids under weather disturbances," *IEEE J. Sel. Topics Appl. Earth Observ.*, vol. 1, no. 3, pp. 170–179, Sep. 2008.

Seme, S., Štumberger, G., Voršič, J., 2011. Maximum Efficiency Trajectories of a Two-Axis Sun Tracking System Determined Considering Tracking System Consumption. *IEEE Trans. Power Electron. 26,* 1280–1290.

Sharma, S.N., 2009. A Kushner approach for small random perturbations of the Duffing-Van der Pol system. *Automatica 45*, 1097–1099.

Shayani, R.A., de Oliveira, M.A.G., 2011. Photovoltaic generation penetration limits in radial distribution systems. *IEEE Trans. Power Syst. 26*, 1625–1631.

Sherwood, L., 2012. U.S. solar market trends 2011. Interstate Renewable Energy Council.

Song, J., Krishnamurthy, V., Kwasinski, A., Sharma, R., 2012. Development of a Markov-chain-based energy storage model for power supply availability of photovoltaic generation plants. *IEEE Trans. Sustain. Energy*, 1 –10.

Stefferud, K., Kleissl, J., Schoene, J., 2012. Solar forecasting and variability analyses using sky camera cloud detection & motion vectors, in: IEEE Power and Energy Society General Meeting. pp. 1– 6.

Taylor, F.J., Mellott, J., 1998. Hands-On Digital Signal Processing. McGraw-Hill Professional Publishing.

Vetterling, W.T., 1992. Numerical Recipes Example Book (C). Cambridge University Press.

ACKNOWLEDGMENTS

The authors acknowledge the assistance of Andrew Dodson, Andrés Escobar, David Guzman, Greg Gambell, Matthew Haase, Daniel Klein, and Corris Stewart.